ACS APPLIED MATERIALS & INTERFACES

Research Article

www.acsami.org

Rigid Origami via Optical Programming and Deferred Self-Folding of a Two-Stage Photopolymer

David J. Glugla,[*,†] Marvin D. Alim,[‡] Keaton D. Byars,[§] Devatha P. Nair,[∥] Christopher N. Bowman,[§] Kurt K. Maute,[⊥] and Robert R. McLeod[†]

[†]Department of Electrical, Computer, and Energy Engineering, University of Colorado, UCB 425, Boulder, Colorado 80309, United States

[‡]Materials Science and Engineering Program, University of Colorado, UCB 596 Boulder, Colorado 80309, United States

[§]Department of Chemical and Biological Engineering, University of Colorado, UCB 596, Boulder, Colorado 80309, United States

[∥]Department of Ophthalmology, University of Colorado Anschutz Medical Campus, Aurora, Colorado 80045, United States

[⊥]Department of Aerospace Engineering, University of Colorado, UCB 429, Boulder, Colorado 80309, United States

Supporting Information

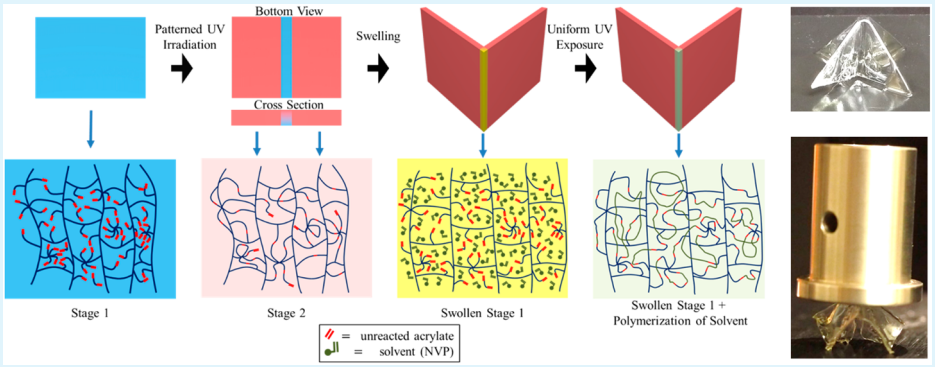

ABSTRACT: We demonstrate the formation of shape-programmed, glassy origami structures using a single-layer photopolymer with two mechanically distinct phases. The latent origami pattern consisting of rigid, high cross-link density panels and flexible, low cross-link density creases is fabricated using a series of photomask exposures. Strong optical absorption of the polymer formulation creates depth-wise gradients in the cross-link density of the creases, enforcing directed folding which enables programming of both mountain and valley folds within the same sheet. These multiple photomask patterns can be sequentially applied because the sheet remains flat until immersed into a photopolymerizable monomer solution that differentially swells the polymer to fold and form the origami structure. After folding, a uniform photoexposure polymerizes the absorbed solution, permanently fixing the shape of the folded structure while simultaneously increasing the modulus of the folds. This approach creates sharp folds by mimicking the stiff panels and flexible creases of paper origami while overcoming the traditional trade-off of self-actuated materials that require low modulus for folding and high modulus for mechanical robustness. Using this process, we demonstrate a waterbomb base capable of supporting 1500 times its own weight.

KEYWORDS: *origami, shape-programmed material, stimuli-responsive materials, folding, polymer sheets, two-stage polymer*

INTRODUCTION

Shape-programmed materials (SPMs) have recently gained popularity as a means for assembling complex 3D structures from 2D sheets.[1−4] The ability to autonomously morph from a 2D sheet into a 3D structure has been used in a myriad of fields including photovoltaics and energy storage,[5,6] microfluidic devices,[7] cell encapsulants and scaffolds,[8−13] surgery,[14] sensing,[15] porous structures and membranes,[16,17] mechanical metamaterials,[18] robotics,[19] and nanooptics.[20,21] At its core, shape-programming involves an initial processing step in which select regions of a sheet are modified to controllably deform upon exposure to an external stimulus at a later time.[1] Polymers are a promising materials system for shape programming due to their wide range of chemical and mechanical properties, large actuation strains in comparison to other active materials,[22] and sensitivity to a variety of external stimuli.[1,23] A common approach toward the patterning of polymer SPMs is to create a sheet out of multiple discrete polymer segments, allowing for regions with dramatically different properties and responses to stimuli. Examples include bilayer,[13,24] trilayer,[25−27] and hinged structures[28,29] whose constituent elements respond differently to heat, solvent, and pH stimuli. Recent work has also

Received: July 21, 2016
Accepted: October 10, 2016
Published: October 19, 2016

DOI: 10.1021/acsami.6b08981
ACS Appl. Mater. Interfaces 2016, 8, 29658−29667

demonstrated the ability to spatially modify and program the mechanical and chemical properties of single-layer, homogeneous polymer films. For example, light absorption within an SU-8 film was used to create a differential cross-link density throughout the thickness, leading to shrinkage-induced bending upon removal of the unreacted material.[30] Other optically patterned properties in single-layer films include differential porosity,[31] alignment of liquid crystal networks,[32,33] shape memory internal stresses,[34] and network relaxation.[26,35] Because these SPMs are fabricated as homogeneous films whose properties are modified by a subsequent optical exposure, they can avoid the complex fabrication steps associated with multilayer material deposition, thereby presenting an attractive means for fabricating complex self-folding 3D structures via simple processing steps.

A popular means for coordinating the stimulus-induced deformations in SPMs utilizes basic origami principles such as creasing and folding, and have been successfully applied to construct 3D devices such as self-folding robots.[36] Creasing occurs during the programming stage of SPMs, and is used to create a pattern of folding hinges and rigid panels. The hinges are characterized by a localized change in the material's mechanical and/or chemical properties such that, upon application of an external stimulus, they selectively undergo directed folding to form the desired 3D structure. Crease panels are those regions that do not respond to the applied stimulus and instead serve to constrain the folding provided by the hinges. Current examples of programmed crease patterns in single-layer SPMs include patterned relaxation of the polymer network using addition−fragmentation chain-transfer (AFT),[35] differential cross-linking to control swelling,[7] mechanical fixing of shape memory polymers,[37,38] and patterned deposition of an infrared-absorptive dye onto a shape memory polymer.[39] Although the above methods all successfully demonstrate the ability to make folded structures from initially homogeneous sheets, some of these techniques require precise control over the applied stimulus in order to produce controlled bending. For example, during thermal triggering of shape memory polymer crease patterns, the glass transition temperature must be exceeded only inside the creased hinges, otherwise the entire structure deforms. Other techniques such as those that rely on AFT processes have not demonstrated the formation of rigid panels, and are therefore limited in the types of structures that they can produce. For example, the Miura-ori pattern and tessellated waterbomb base, which exhibit negative Poisson's ratio and reduced degrees of freedom, are two of the most common origami structures used in engineering applications.[40] However, without the constraints imposed on the folds by rigid panels, the structures lose these unique mechanical properties. Finally, the inability of some of the aforementioned programming techniques to harden the flexible hinges after folding limits the ultimate rigidity and stability of the end product, thereby restricting its use as a load-bearing structure.

Using a two-stage photopolymer system, we characterize and demonstrate an easily processed, single-layer, 2D SPM capable of folding into permanent, 3D, load-bearing structures. Latent crease pattern hinges and panels are independently programmed into the initial loosely cross-linked and rubbery stage 1 material via a series of optical exposures controlled by photomasks. The first exposure step creates the rigid, stage 2 panels by applying a large optical exposure dose to both sides of the material, while the unexposed hinges remain flexible and rubbery. A second photomask exposure applied to the bottom and top side of the photoabsorptive sheet programs mountain and valley folds respectively by creating a depth-wise gradient in the cross-link density of the hinges. Upon immersion of the flat sheet into a polymerizable solvent, these patterned hinges undergo nonuniform swelling, causing the mountain and valley folds to actuate, and the sheet to transform into the programmed 3D structure. After swelling, a final, uniform exposure step permanently fixes the shape via photopolymerization of both the monomeric solvent and unreacted stage 1 material. This last exposure increases the final modulus and glass transition temperature of the hinges by more than an order of magnitude compared to the stage 1 material, thereby forming a rigid, permanent structure capable of supporting external loads up to 1500 times its own weight.

EXPERIMENTAL SECTION

Two-Stage Polymer. The two-stage polymer was adopted from the procedure developed by Nair et al.[41,42] The thiol monomer, trimethylolpropane tri(3-mercaptopropionate) (Thiocure TMPMP) was donated by Bruno Bock. The acrylate monomers used were hexafunctional aliphatic urethane acrylate oligomers (Ebecryl 1290) and difunctional tricyclodecane dimethanol diacrylate (TCDDA), donated by Allnex and Sartomer, respectively. The UV photoinitiator DMPA (2,2-dimethoxy-2-phenylacetophenone) was donated by Ciba Specialty Chemicals, and the UV absorber, Tinuvin 328 was purchased from CIBA. The base used to catalyze the thiol-Michael reaction, triethyl amine (TEA), was purchased from Sigma-Aldrich. To provide a large difference in mechanical properties between stage 1 and 2, we fabricated samples with a 2:1 ratio of acrylate to thiol functional groups, and a 1:1 ratio of hexacrylate to diacrylate functionalities. In all samples, 2.5 wt % of TEA and 1 wt % DMPA were added to initiate the stage 1 and stage 2 reactions, respectively. To make the polymer, we initially mixed together the photoinitiator and thiol, and then added them to the acrylates. Mixing during each step was performed in a heated (65° C) water bath. TEA was added after all other materials were evenly mixed in order to catalyze the stage 1 thiol-Michael polymerization. Sheet thickness was controlled by casting the material between two silanated (RainX) glass plates with 127 or 254 μm spacers. A small amount of the material was also cast between salt plates and monitored via Fourier-Transform Infrared Spectroscopy (FTIR) to ensure full conversion of the thiol groups. Upon completion of the thiol-Michael reaction, the polymer sheet was delaminated from the plates and cut into various geometries for testing. For the creation of 3D, self-actuating folds and bends, 0.5 wt % of Tinuvin 328 was added to attenuate light intensity through the 127 μm thick sample. N-Vinyl-2-pyrrolidone (NVP) (Acros Organics) mixed with 2 wt % of the photoinitiator 2, 4, 6-trimethylbenzoyldiphenylphosphine oxide (TPO) was used as the photopolymerizable solvent to swell and fold the creased materials.

Optical Exposure Conditions. After completion of the thiol-Michael stage 1 reaction, samples were delaminated from the glass plates and exposed directly to 365 nm light at 5 mW/cm^2 using an EXFOS Acticure 4000, 100 W high pressure mercury lamp equipped with a 365 nm bandpass filter. The relative stage 2 conversion was controlled by varying the exposure time, with longer exposure times facilitating higher stage 2 acrylate conversions. All irradiated samples were stored in the dark for at least 3 h to allow any ongoing reactions to terminate, and to stabilize the network.

To polymerize the NVP/TPO solution and fix the shape of the swollen, folded structures, we used 11 mW/cm^2, 365 nm light to uniformly expose the material from each side. Exposure times of 90 s for each side were used in all cases.

Fourier Transform Infrared Spectroscopy. FTIR spectroscopy was used to monitor the homopolymerization of the remaining unreacted acrylates during stage 2 curing. A Thermo Scientific Nicolet 6700 FTIR spectrometer was fitted with a specialty mount for simultaneous UV irradiation, which allowed for monitoring of the acrylate peak at 814 cm^{-1} and concurrent irradiation of the sample

DOI: 10.1021/acsami.6b08981
ACS Appl. Mater. Interfaces 2016, 8, 29658−29667

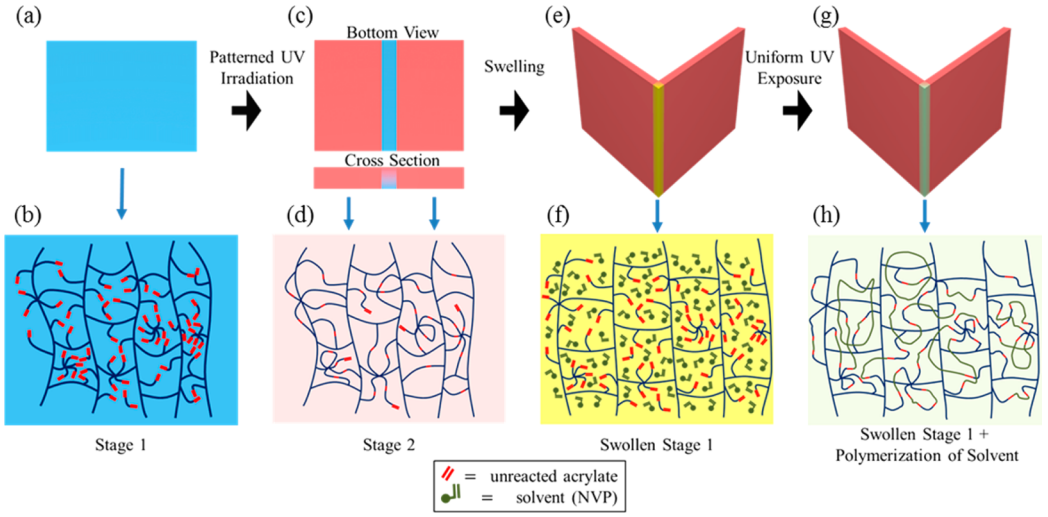

Figure 1. Overall scheme depicting the different material states accessible to the two-stage photopolymer, and their application for creating self-folding SPMs. (a, b) Initial stage 1 material (blue) is composed of a rubbery and loosely cross-linked thiol−acrylate matrix with excess unreacted acrylate groups. (c, d) After exposure to UV light, the excess unreacted acrylates in the stage 1 material react to form a rigid, high-cross-link stage 2 matrix (red). Addition of a photoabsorber in the material allows for a gradient between stage 1 and 2 to be formed within the thickness of the material. (e, f) Upon immersion in N-Vinyl-2-pyrrolidone (NVP), the stage 1 material swells (yellow). This swelling can be combined with the gradient-patterned material to create a self-folding hinge. (g, h) After folding, the swollen material is exposed to UV light, causing the NVP and unreacted acrylates to polymerize, resulting in a rigid, permanently swollen matrix (green).

with 5 mW/cm^2, 365 nm light. Optically transparent samples were prepared between two salt (NaCl) plates and allowed to cure at ambient temperature via the thiol-Michael reaction for 24 h. Completion of the thiol-Michael stage 1 reaction was determined by ensuring that no remaining thiol peak around 2550 cm^{-1} was present. Then, the final conversion of the remaining unreacted acrylates (c_{acrylate}) was monitored by integrating the peak over the range 790−830 cm^{-1} for varying exposure times and intensities. The area of the acrylate peak upon completion of the stage 1 reaction was given by A_{initial}, and A_{final} was the area under the acrylate peak after completion of the stage 2 photoinitiated acrylate homopolymerization.

$$c_{\text{acryalte}} = 1 - \left(\frac{A_{\text{final}}}{A_{\text{initial}}}\right)$$

Swelling Strain vs Dose. Bulk swelling measurements were performed by immersing 127 μm thick, 6.35 mm radius discs of the optically thin two-stage polymer into NVP. Uniform cross-link density was achieved by preparing the polymer discs without photoabsorber. Once the samples reached equilibrium swelling strain after 24 h, they were removed from the solvent and patted dry to remove any excess liquid on the surface. Pictures of the new, swollen discs were taken, and their corresponding radii were computed using ImageJ software and the ThreePointCircularROI plugin developed by Gabriel Landini.[43]

Tensile Testing. The tensile modulus of the polymer strips vs optical exposure dose was measured using a TA Instruments Q800 DMA. Strips without photoabsorber were cut into rectangles measuring 6.35 × 12.7 × 0.127 mm, exposed with 5 mW/cm^2, 365 nm light, and then strained at a rate of 800 μm/min at room temperature (23 °C) in order to obtain the elastic stress−strain curve. When measuring the swollen modulus, strips prepared without photoabsorber were first irradiated with 5 mW/cm^2, 365 nm light, and then set aside for at least 3 h to allow for the completion of dark polymerization. The samples were then immersed in the NVP solvent for 24 h. Immediately prior to measuring the stress−strain curve, the samples were removed from the solvent and patted dry.

Cross-Link Density and Glass-Transition Temperature. To measure the cross-link density and glass-transition temperature (T_g) of the material as a function of optical exposure dose, we first exposed unswollen, stage 1 samples prepared without photoabsorber, with dimensions of 10 × 6 × 0.25 mm with 5 mW/cm^2, 365 nm light, and then stored them in the dark for at least 3 h. Measurements were obtained using a TA Instruments Q800 DMA. The sample temperature was ramped at 3 °C/min from −20 to 180 °C with a frequency of 1 Hz and strain of 0.0125% in tension. The T_g was assigned as the maximum of the tan δ curve after a single temperature scan, and the cross-link density ($\rho_{\text{cross-link}}$) for each sample was calculated using the following equation[44]

$$\rho_{\text{cross-link}} = \frac{E'}{3RT}$$

where R is the gas constant and E' is the storage modulus at temperatures $T = T_g + 50$ °C.

A similar method was used to determine the T_g of strips that were first swollen with the NVP/TPO solution and then uniformly exposed with 365 nm light. In this case, the stage 1 material was swollen in the NVP/TPO solution for 24 h and then exposed on both sides with 11 mW/cm^2 light at a dose of 990 mJ/cm^2. The T_g was then measured using the same Q800 DMA and parameters as before.

Bend Radius of Curvature. Two-stage polymer containing 0.5 wt % Tinuvin 328 was cut into strips measuring 6.35 × 1.6 × 0.127 mm. Each strip was then exposed for different amounts of time using 365 nm light at 5 mW/cm^2. After exposure, the strips were stored in the dark for 3 h to allow for completion of dark polymerization prior to immersion in the NVP solvent. Measurements of the bend radius of curvature were taken after 24 h of swelling. Images of the strips were captured and the bend radius was analyzed using ImageJ software and the ThreePointCircularROI plugin.[43]

RESULTS AND DISCUSSION

Synthesis and Characterization of Dual Cure Sheets. The two-stage polymer uses orthogonal polymerization reactions to produce a material with two sets of distinct mechanical properties (Figure 1). The stage 1 network is designed to have a low modulus and be loosely cross-linked, whereas the photoinitiated stage 2 reaction is designed to produce a network with a modulus and cross-link density that are at least an order of magnitude higher. A thiol-Michael base-catalyzed polymerization reaction is used for the stage 1 polymerization, while stage 2 is induced via a photoinitiated chain-growth acrylate homopolymerization. Photoinitiated

DOI: 10.1021/acsami.6b08981
ACS Appl. Mater. Interfaces 2016, 8, 29658−29667

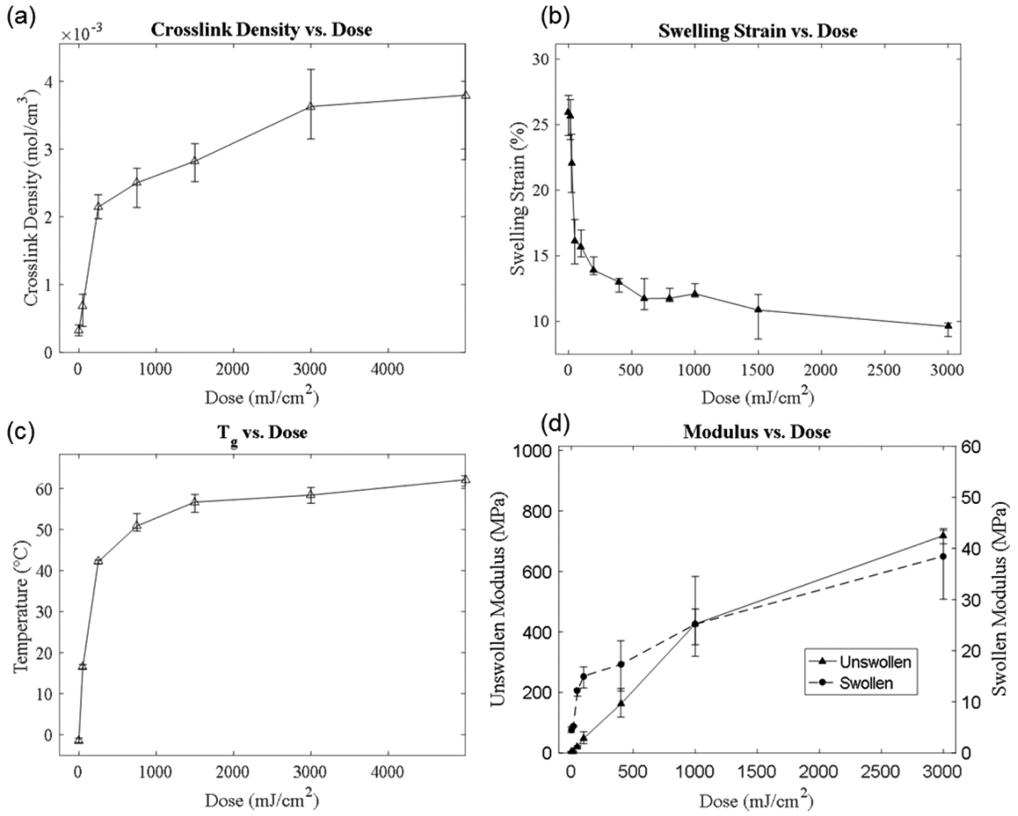

Figure 2. All exposures were performed using an intensity of 5 mW/cm^2 at 365 nm. By controlling the applied irradiation dose at a single intensity, mechanical properties of the polymer may be set anywhere between those of the stage 1 (low dose) and 2 (high dose) networks. (a) Cross-link density of the stage 2 network is roughly an order of magnitude larger than at stage 1. (b) Upon immersion in a solvent, the maximum difference in swelling strain between the stage 1 and 2 networks is about 16%. (c) Glass transition temperature of the stage 1 network is well-below room temperature, whereas the stage 2 network possesses a glass transition well above room temperature. (d) Tensile modulus of both the unswollen and swollen network (in NVP) is at least an order of magnitude larger in stage 2 as compared to stage 1.

polymerization in the stage 2 reaction allows for selective spatial patterning of the stage 2 properties throughout the material. In order to produce a wide range of mechanical properties between stage 1 and 2, the initial stage 1 network is fabricated using a 2:1 ratio of acrylate to thiol functional groups, allowing for the large excess concentration of acrylates needed in the stage 2 reaction (Figure 1b). The acrylate mixture is a 1:1 ratio by functional group of di- and hexacrylates to allow for the formation of both the low and high cross-link density networks. Furthermore, the lower molecular weight of the diacrylate facilitates mixing of the initial thiol−acrylate solution by lowering the viscosity of the mixture of monomers.

Due to the relatively low concentration of thiol functional groups, the stage 1 material forms a flexible, loosely cross-linked network (4×10^{-3} mol/cm^3) with a T_g well-below room temperature (−8 °C), and a modulus of around 4 MPa (Figure 2a, c, d). Because of the low cross-link density, the stage 1 sheet can readily absorb NVP, resulting in swelling strains of up to 26% (Figure 2a, b).

The second stage reaction of the material is accessed via irradiation with UV light, which triggers a chain-growth homopolymerization of the residual unreacted acrylate groups that remain after the stage 1 reaction. Maximum conversion of the residual acrylate bonds, as measured via FTIR, peaks at ∼70% and is attributed to the decreased mobility of the acrylates as the network cross-link density increases.[41,45] At the point of maximum conversion, the resulting cross-link density increases by an order of magnitude compared to the stage 1 network (Figure 2a). As a result, the T_g moves to well-beyond room temperature, and the tensile modulus increases by roughly 2 orders of magnitude (Figure 2c, d). The increased cross-link density reduces the amount of solvent uptake, restricting the sheet to undergo only 10% swelling strain when immersed in the NVP solvent (Figure 2b). In photoinitiated chain-growth polymerizations, the extent of conversion, and thus increase in tensile modulus, cross-link density, and glass-transition temperature, monotonically increases with the number of generated radicals. However, the number of these generated radicals is often nonlinearly dependent on the exposure intensity. Thus, for this proof-of-concept study, intermediate mechanical properties between the two stages are achieved by carefully controlling the applied exposure intensity and dose, and preserving the samples in the dark at ambient conditions in order to stabilize them (Figure 2).

Solvent evaporation imposes a significant limitation on self-folding structures that utilize swelling-induced actuation. Because of evaporation, the resulting swollen structures are vulnerable to a wide range of environmental conditions such as heat and vacuum. However, the solvent used in the proposed material system is chosen to be a polymerizable monomer/photoinitiator solution consisting of NVP and TPO, such that a uniform light exposure applied immediately after folding polymerizes the monomer. This polymerization step permanently locks the now polymerized solvent into the structure while concurrently mechanically reinforcing the swollen hinges. To quantify this stiffening effect in the hinge regions, initially

DOI: 10.1021/acsami.6b08981
ACS Appl. Mater. Interfaces 2016, 8, 29658−29667

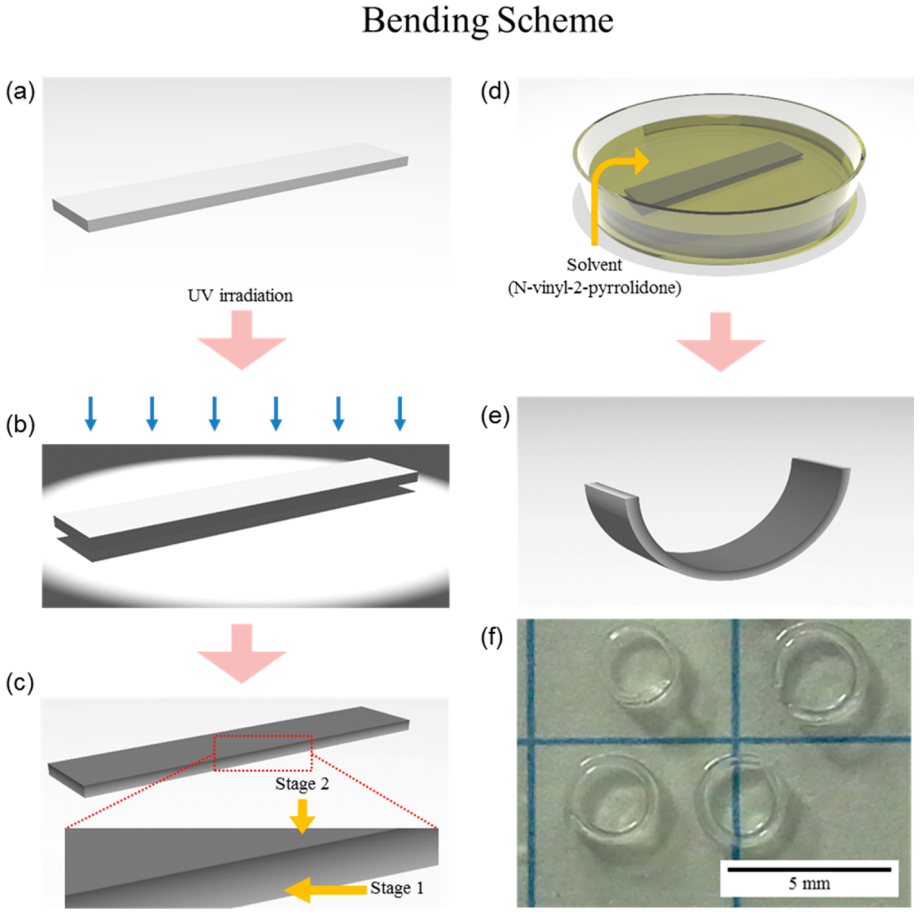

Figure 3. Scheme used to induce bending in the two-stage polymer. (a, b) Strip fabricated with absorber is irradiated by 365 nm light,(c) creating a gradient in the cross-link density and modulus through the thickness of the material. (d, e) Upon immersion in a solvent (N-Vinyl-2-pyrrolidone), the gradient in cross-link density causes the strip to differentially swell, inducing bending. (f) Side-view of the bent strips after removal from the solvent.

unexposed polymer strips were swollen in the NVP/TPO solution and then exposed with 11 mW/cm^2, 365 nm light using doses of 990 mJ/cm^2 on each side. Photopolymerization of the solvent increases the tensile modulus of the swollen strip to ~790 MPa, and the T_g of the material to 130 °C, which is well above the maximum T_g of either the stage 1 or stage 2 networks (Figure 2c). Through this stiffening process, rigid, folded 3D structures may be formed.

Bending the Two-Stage Material. Bending of a two-stage polymer strip is achieved by inducing a depth-wise gradient in the mechanical properties via a single-sided optical exposure (Figure 3a–c). Immersion of the sheet in a favorable solvent then causes the material to undergo differential swelling and bending (Figure 3d–f).

A qualitative understanding of the factors that control this bending is given by the composite beam theory.[46] Because the length to thickness ratio of the samples is 50, the strips are considered slender, and a simple Euler–Bernoulli model is applicable. Using these assumptions, the bend radius at the center of a thin composite beam subject to differential axial expansion across its thickness is given by

$$\frac{1}{\rho} = \frac{\int_0^h E\epsilon(z - z_N)\mathrm{d}z}{\int_0^h E(z - z_N)^2\mathrm{d}z}$$

where ρ is the radius of curvature (ROC), z is the coordinate along the thickness direction, h is the total thickness of the strip, E is swollen tensile modulus, ϵ is the swelling strain, and z_N is the location of the neutral axis computed as follows: $z_N = \int_0^h Ezdz/\int_0^h Edz$. The numerator in the equation above represents the bending moment created by the differential swelling, while the denominator characterizes the bending stiffness. The tensile modulus and the swelling strain depend on the exposure dose, as shown in Figure 2. Because of the Beer–Lambert law, the incident light intensity undergoes a smooth, exponential decay as it passes through the material, resulting in a depth-dependent dose. Additionally, processes such as saturation of the material response, and a polymerization rate that is sublinear with intensity further alter the resulting distribution of mechanical properties throughout the strip. Thus, a direct mapping between the mechanical properties and the applied dose without accounting for the light intensity should not be used. To obtain a more accurate estimate of the distribution of material properties across the thickness of the strip, and to improve the bend ROC prediction, the data shown in Figure 2 is mapped to an "effective dose" (D_{eff_cal}) that accounts for the sublinear dependence of the polymerization rate on intensity. This sublinear dependence with intensity arises from the dominance of bimolecular termination during the polymerization reaction, whereby the polymerization rate scales with the square root of the light intensity (see the

DOI: 10.1021/acsami.6b08981
ACS Appl. Mater. Interfaces 2016, 8, 29658–29667

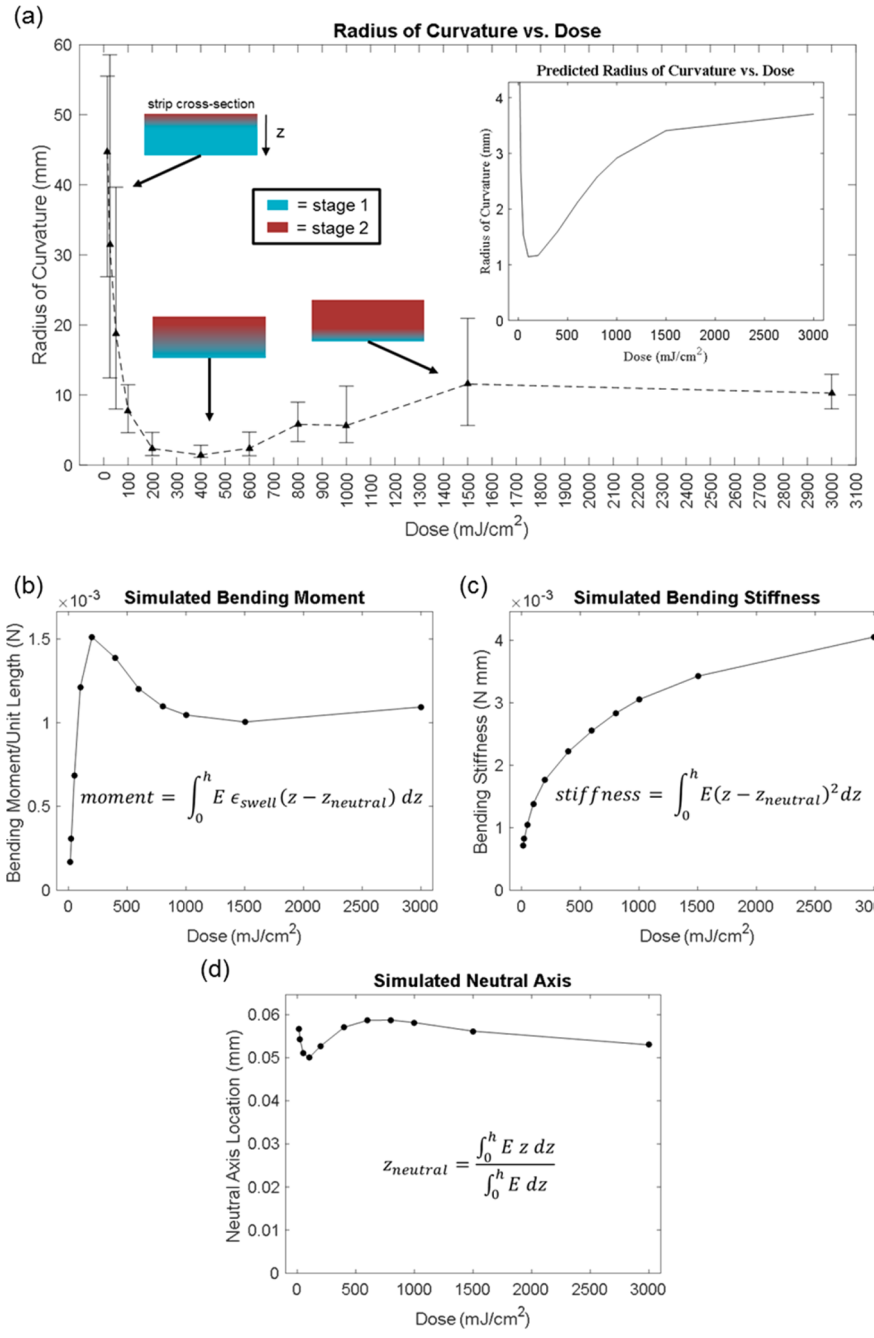

(e)

Solvent: N-Vinyl-2-Pyrrolidone	Pre-Flood Cure	Post-Flood Cure	% Increase
Radius of Curvature (mm)	1.52	2.02	33.0%

Figure 4. (a) Radius of curvature (ROC) for 6.4 × 1.6 × 0.13 mm strips as a function of exposure dose at 5 mW/cm^2, 365 nm light. The error in ROC measurements becomes large as ROC ≫ strip length. (Inset) Estimated ROC using the Euler−Bernoulli composite beam model. (b−d) Simulated bending moment, bending stiffness, and neutral axis vs front exposure dose using the Euler−Bernoulli composite beam model. (e) Radius of curvature increases by up to 33% after the final uniform exposure to polymerize the NVP.

Supporting Information). Thus, $D_{\text{eff\_cal}} = t\sqrt{I}$ is the product of the exposure time (t) and square root of the light intensity (I). The effective dose as a function of depth within the strip, $D_{\text{eff\_strip}}(z)$, is then calculated by first using the Beer−Lambert law to determine the depth-wise intensity profile ($I(z)$) and then multiplying by the exposure time. Interpolation of the mapped data from Figure 2 using $D_{\text{eff\_strip}}(z)$ then yields the resulting material properties as a function of depth within the strip

$$E(z) = E(D_{\text{eff\_strip}}(z)) \text{ and } \epsilon(z) = \epsilon(D_{\text{eff\_strip}}(z))$$

with

$$D_{\text{eff\_strip}}(z) = t\sqrt{I(z)};\ I(z) = I_0 e^{-\log(10)A(z)};\ A(z) = \epsilon c z$$

DOI: 10.1021/acsami.6b08981
ACS Appl. Mater. Interfaces 2016, 8, 29658−29667

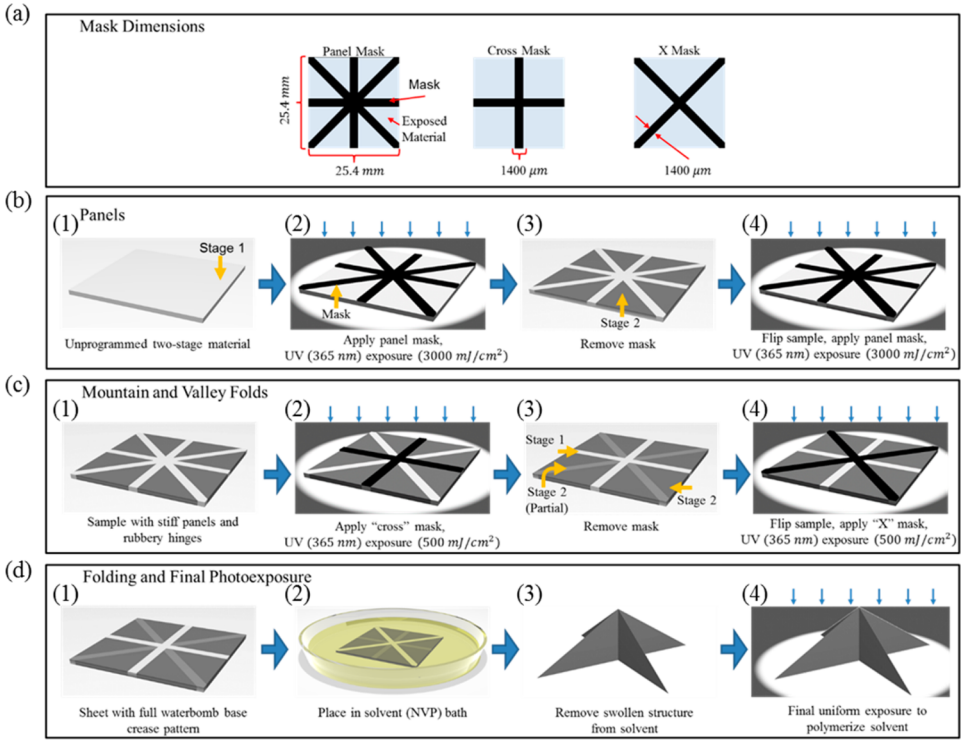

Figure 5. (a) Masks used to create the waterbomb base structure. Creasing and folding the waterbomb base involves 3 main processing steps: creating the stiff panels, programming the mountain and valley folds, and folding the final structure. (b) Hardening of the panels is performed using large exposure doses applied to each side of the sheet through the panel mask. (c) Mountain and valley folds are created by applying either the "cross" or "X" mask to a single side and using a small exposure dose. Both types of folds may be programmed into the same sheet by applying the two masks to different sides. (d 1–2) Folding of the creased structure occurs upon immersion into a solvent. (d 3–4) Fnal uniform cure applied to each side of the structure is used to polymerize the solvent and make the final structure permanent.

where I_0 is the incident light intensity at the illuminated surface of the strip, $A(z)$ is the depth-dependent material absorbance, ϵ is the molar absorptivity of the material, and c is the concentration of absorber. For the z = 127 μm thick strip, $A(z = 127\ \mu\text{m}) = 2.3$ at 365 nm. Note that the z-coordinate is zero at the illuminated surface.

Experimental results for the bend ROC vs applied dose at the front surface of an isolated 6.35 × 12.7 × 0.127 mm strip are shown in Figure 4a. The incident light intensity was 5 mW/cm^2 for all samples. ROC results predicted by the simple beam theory outlined above are also shown in the inset of Figure 4a. The beam theory qualitatively matches the experimental measurements, and, aside from differences in ROC values, provides insight into the interplay between bending stiffness and bending moment, and their effect on the resulting ROC. The computed bending stiffness, bending moment, and location of the neutral axis as a function of applied exposure dose are shown in Figure 4b–d, whereas the associated depth profiles of the tensile modulus and swelling strain at select doses are shown in the Supporting Information. Although the tensile modulus, and therefore bending stiffness, increase monotonically with the exposure dose, the bending moment and the location of the neutral axis exhibit a more complex relationship with the exposure dose. However, regardless of the applied dose, the location of the neutral axis experiences only small shifts and remains below $z < h/2 = 63.5\ \mu$m. At small doses below 100 mJ/cm^2, the top surface receives an insufficient exposure dose to induce significant conversion to stage 2. For these conditions, the difference in swelling strain and tensile modulus about the neutral axis of the strip is small. Thus, the ensuing bending moment is too weak relative to the bending stiffness to deform the beam, resulting in a large ROC. As the exposure dose increases to 100 mJ/cm^2, the front surface is converted to stage 2, whereas the back surface, receiving little light because of the absorber, remains at stage 1. Initially, this difference in both the swelling strain and tensile modulus about the neutral axis causes the bending moment to grow faster than the bending stiffness, thereby decreasing the ROC. Beyond doses of 100 mJ/cm^2, the neutral axis is slightly shifted toward the illuminated surface, indicating an increased difference in tensile modulus between the front and back sides, and even greater conversion of the front surface toward stage 2. This difference in the mechanical properties of the strip about the neutral axis leads to a peak in the bending moment around a dose of 200 mJ/cm^2. However, because of continued conversion, the difference in the product of the tensile modulus and swelling strain about the neutral axis then decreases, causing the bending moment to experience a small drop, which when combined with the increase in bending stiffness results in an increase of the ROC. Because of the significant attenuation of light intensity at the back surface of the strip, conversion of the back surface toward stage 2 is slow and the difference in swelling strain and tensile modulus about the neutral axis remains relatively unchanged over the dose range of interest, causing the bending moment to plateau. For an infinite dose, the material would eventually convert to stage 2 and the uniformity in material properties throughout the depth would cause both the neutral axis to shift to the middle of the strip, and the bending moment to fall back to 0.

DOI: 10.1021/acsami.6b08981
ACS Appl. Mater. Interfaces 2016, 8, 29658–29667

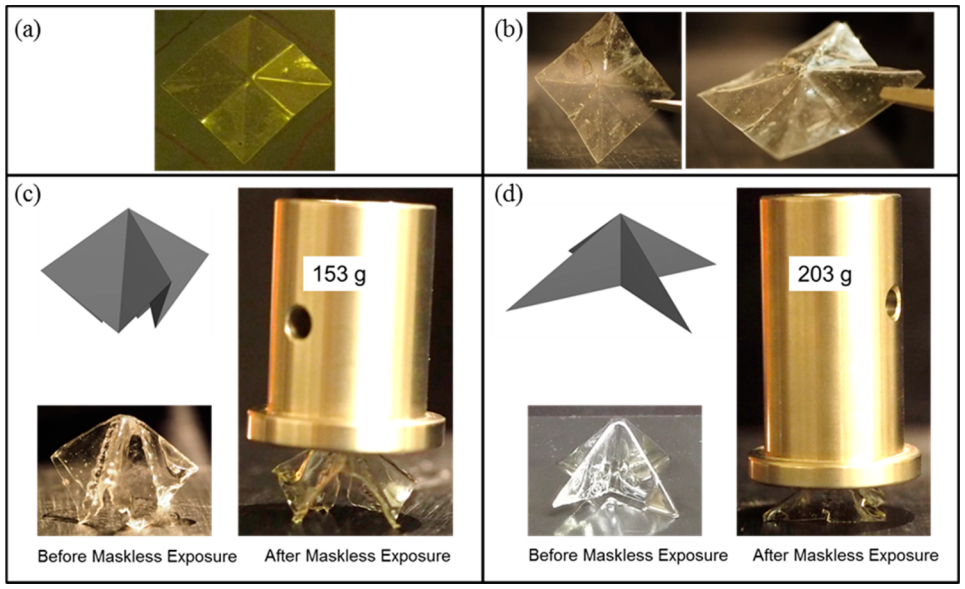

Figure 6. (a) Unswollen two-stage polymer sheet that has been programmed with the waterbomb base crease pattern. (b) If solvent is allowed to evaporate from the folded structure, it will return to a flat sheet. Because of the bistability of the waterbomb base, folding the creased pattern produces 2 different structures. (c,d) Two different bistable states of the waterbomb base are shown along with the experimentally achieved folded structure. If a uniform light exposure is applied to the folded structure immediately after swelling, the structure's rigidity increases and is capable of supporting an external load whose maximum weight depends on the selected bistable structure. The structure in c is capable of supporting a maximum load up to 1140 times its own weight, whereas the structure in d is capable of supporting up to 1500 times its own weight.

Overall, the minimum ROC predicted using the simplified beam model and the given experimental parameters is 1.4 mm, or ∼11 times the strip thickness, which equates to a factor of 1.4 smaller than the minimum measured ROC (2.0 mm) for the chosen material and strip dimensions. Using a more sophisticated nonlinear finite element model with a Neo-Hookean constitutive material model yields a slightly better prediction of ROC vs applied dose than the simple Euler–Bernoulli model, however, the same qualitative trend in the ROC is observed (see the Supporting Information).

After bending the strip, a final, uniform exposure polymerizes the monomeric solvent and fixes the shape of the bent structure. As shown in Figure 4e, shrinkage resulting from polymerization of the NVP solvent and remaining unreacted stage 1 acrylates causes the resulting bend radius to increase by up to 33%.

Folding 3D Structures. Unlike bending, where the entire sheet is subject to the swelling response, folding occurs via localized bending of flexible hinges surrounded by stiff panels. In origami, a crease pattern is imposed into an otherwise rigid sheet, creating the flexibility required for the folding hinges while maintaining stiff panels for mechanical strength of the final folded object. To demonstrate the capability to pattern folds into the two-stage polymer, we programmed a waterbomb base crease pattern utilizing both mountain and valley origami folds into a 25.4 × 25.4 × 0.127 mm sheet of the material using the process outlined in Figure 5.

The folded structure is created using 3 sequential exposure steps that (1) define the stiff panels, (2) define the mountain and valley folds, and (after swelling and folding) (3) lock-in the permanent shape of the folded structure. Stiff panels with a high modulus and cross-link density throughout their thickness are programmed via high-dose, photomask exposures applied from both sides of the material (Figure 5b 1–4). The resulting sheet possesses two mechanically distinct regions featuring the stiffened, rigid panels (stage 2 material) and flexible hinges (stage 1 material) (Figure 5c 1). Mountain or valley folds are then created via small-dose, single-sided mask-exposures applied to select hinges (Figure 5c 2–4). The small exposure dose establishes a gradient in the mechanical properties that causes nonuniform swelling of the hinge, leading to directed bending/folding. Because these folds remain latent until triggered by solvent, programming of both the mountain and valley folds may be performed on the same 2D surface through masked exposures applied to either side of the sheet. Control over both the width of the hinge and the mechanical gradient is possible by adjusting the mask and exposure dose, respectively. After patterning the creases, immersion into a monomeric solvent (NVP) initiates the latent crease program and causes the structure to autonomously fold (Figure 5d 1–3). A final uniform optical exposure applied to the front and back of the structure polymerizes both the remaining unreacted stage 1 acrylates as well as the NVP solvent, thereby stiffening the hinges and raising the modulus of the entire structure (Figure 5d 4). Because of the polymerization of the solvent within the material, evaporation does not occur, and the structure's shape becomes permanent.

An example of the preprogrammed, unfolded waterbomb base is shown in Figure 6a. The panels were exposed using 365 nm light from each side with a dose of 3000 mJ/cm^2 at an intensity of 5 mW/cm^2, while the mountain and valley folds were each exposed to 500 mJ/cm^2 on a single side. Optimal hinge width to achieve the sharpest folds was 1.4 mm. Although the preprogrammed sheet exhibits weak bending in the hinges because of polymerization-induced shrinkage from stage 1 to stage 2, the material remains sufficiently flexible to be pressed against the exposure mask during all programming steps. The folded structure, prior to the final uniform exposure step, is shown in (Figure 6c, d). In contrast to the isolated bend structures measured in the previous section, the bend radii exhibited by the hinges in the waterbomb base are as small as 0.5 mm. This difference in bending is found to be primarily

DOI: 10.1021/acsami.6b08981
ACS Appl. Mater. Interfaces 2016, 8, 29658–29667

caused by assistance from swelling-induced buckling in the unexposed vertex at the center of the sheet (see the Supporting Information). As the vertex swells, it is constrained by the rigid panels and is forced to buckle along the hinges. Such buckling assists the folding process in each hinge and promotes a tighter bend radius than that which is normally achieved in an isolated hinge. This assisted folding is made possible by the interaction between the stiff panels and the flexible material at the vertex. For entirely flexible materials with no stiff regions, such buckling does not occur, and the structure will not fold as tightly.

Evaporation of the NVP solvent causes the folded waterbomb base to eventually return to a flat sheet (Figure 6b). However, a uniform flood exposure applied immediately after the structure is removed from the NVP bath, before evaporation can occur, causes polymerization of the swollen NVP and locks in the shape of the structure while concurrently reinforcing the hinges. Although some polymerization shrinkage causes the hinges to open and the panel edges to curl, the final shape remains comparable to the initial folded structure. Due to the extra polymerization step, the tensile modulus and T_G of the polymer structure's hinges greatly increase, reaching values as high as 790 MPa and 130 °C respectively, thereby allowing the structure to support an external load. This was demonstrated by applying a series of increasing weights to the structure, with the maximum loading weights shown in Figure 6c, d. The maximum recoverable loading of the flood-cured, 0.134 g waterbomb base is 203 g, which is ∼1500 times its own weight. It is important to note that the geometry of the waterbomb base crease pattern allows for two different stable structures[47] (Figure 6c, d) which arise from the single degree of freedom allowed by the flexible, unpatterned material at the vertex of the mountain and valley folds in the center of the square sheet. Due to their final geometries, the maximum supportable load of these two bistable structures is different. The structure in Figure 6c, which is only supported by 4 narrow points, can bear up to 1140 times its weight, whereas the alternate structure in Figure 6d, which is instead supported by the edges of the polymer sheet, can support up to 1500 times its own weight.

CONCLUSION

Origami allows for the formation of complex, mechanically interesting 3D structures from 2D sheets using preprogrammed crease patterns consisting of flexible hinges and rigid panels. A two-stage photopolymer system is presented as an advantageous material for creating such crease patterns due to its ability to exhibit both flexibility and rigidity in a single sheet at different times and 3D locations under precise optical control. With the addition of an optical absorber, the two-stage material is capable of undergoing three distinct patterning modalities that are amenable to the creation of permanent, rigid origami structures: (1) uniform patterning in depth to produce stiff, rigid panels; (2.) strong gradients in depth to create directed self-folding hinges; and (3) permanent fixation of the final structure's shape via a uniform optical exposure. The latent nature of the crease pattern allows all processing to be performed on the 2D sheet using mask lithography, while actuation occurs at a later time through application of an external stimulus. Using these steps, we demonstrate the ability to fabricate a self-folding, permanent, rigid waterbomb base capable of supporting loads up to 1500 times its own weight. We also observe that constrained swelling imposed by the rigid panels on the unpatterned regions can be used to assist the bending of hinges and enhance the overall folding of the programmed crease pattern. In the waterbomb base structure, constrained swelling of the central unpatterned vertex allows for bend radii that are a factor of 3 smaller than isolated bends created on individual strips. In summary, the combination of a two-stage polymer and facile optical programming demonstrated herein enables stiff panels separated by mountain and valley creases that undergo folding and final hardening in response to simple, delayed external stimuli. These features enable complex patterns of sharp folds in otherwise flat sheets to create mechanically and environmentally robust final parts, avoiding the common issues of precise stimulus control, pliable final state, and impermanent shape.

ASSOCIATED CONTENT

Supporting Information

The Supporting Information is available free of charge on the ACS Publications website at DOI: 10.1021/acsami.6b08981.

Additional information for predicting the mechanical properties within the UV-exposed absorptive strip, and a comparison of the bend radius of curvature predicted using the Euler−Bernoulli composite beam model and the nonlinear finite element model with a Neo-Hookean constitutive material model (PDF)

AUTHOR INFORMATION

Corresponding Author

*E-mail: david.glugla@colorado.edu.

Notes

The authors declare no competing financial interest.

ACKNOWLEDGMENTS

The authors are grateful to the National Science Foundation (EFRI-1240374) for providing funding for this research.

REFERENCES

(1) Liu, Y.; Genzer, J.; Dickey, M. D. 2D or Not 2D": Shape-Programming Polymer Sheets. *Prog. Polym. Sci.* **2016**, *52*, 79−106.

(2) Geryak, R.; Tsukruk, V. V. Reconfigurable and Actuating Structures from Soft Materials. *Soft Matter* **2014**, *10* (9), 1246−1263.

(3) Studart, A. R.; Erb, R. M. Bioinspired Materials That Self-Shape through Programmed Microstructures. *Soft Matter* **2014**, *10* (9), 1284−1294.

(4) Peraza-Hernandez, E. A.; Hartl, D. J.; Malak, R. J., Jr; Lagoudas, D. C. Origami-Inspired Active Structures: A Synthesis and Review. *Smart Mater. Struct.* **2014**, *23* (9), 094001.

(5) Guo, X.; Li, H.; Ahn, B. Y.; Duoss, E. B.; Hsia, K. J.; Lewis, J. A.; Nuzzo, R. G. Two- and Three-Dimensional Folding of Thin Film Single-Crystalline Silicon for Photovoltaic Power Applications. *Proc. Natl. Acad. Sci. U. S. A.* **2009**, *106* (48), 20149−20154.

(6) Bof Bufon, C. C.; Cojal González, J. D.; Thurmer, D. J.; Grimm, D.; Bauer, M.; Schmidt, O. G. Self-Assembled Ultra-Compact Energy Storage Elements Based on Hybrid Nanomembranes. *Nano Lett.* **2010**, *10* (7), 2506−2510.

(7) Jamal, M.; Zarafshar, A. M.; Gracias, D. H. Differentially Photo-Crosslinked Polymers Enable Self-Assembling Microfluidics. *Nat. Commun.* **2011**, *2*, 527.

(8) Huang, G.; Mei, Y.; Thurmer, D. J.; Coric, E.; Schmidt, O. G. Rolled-up Transparent Microtubes as Two-Dimensionally Confined Culture Scaffolds of Individual Yeast Cells. *Lab Chip* **2009**, *9* (2), 263−268.

(9) Zakharchenko, S.; Puretskiy, N.; Stoychev, G.; Stamm, M.; Ionov, L. Temperature Controlled Encapsulation and Release Using Partially

DOI: 10.1021/acsami.6b08981
ACS Appl. Mater. Interfaces 2016, 8, 29658−29667

Biodegradable Thermo-Magneto-Sensitive Self-Rolling Tubes. *Soft Matter* **2010**, *6* (12), 2633−2636.
(10) Zakharchenko, S.; Sperling, E.; Ionov, L. Fully Biodegradable Self-Rolled Polymer Tubes: A Candidate for Tissue Engineering Scaffolds. *Biomacromolecules* **2011**, *12* (6), 2211−2215.
(11) Jamal, M.; Bassik, N.; Cho, J.-H.; Randall, C. L.; Gracias, D. H. Directed Growth of Fibroblasts into Three Dimensional Micropatterned Geometries via Self-Assembling Scaffolds. *Biomaterials* **2010**, *31* (7), 1683−1690.
(12) Bassik, N.; Stern, G. M.; Jamal, M.; Gracias, D. H. Patterning Thin Film Mechanical Properties to Drive Assembly of Complex 3D Structures. *Adv. Mater.* **2008**, *20* (24), 4760−4764.
(13) Stoychev, G.; Puretskiy, N.; Ionov, L. Self-Folding All-Polymer Thermoresponsive Microcapsules. *Soft Matter* **2011**, *7* (7), 3277−3279.
(14) Gultepe, E.; Randhawa, J. S.; Kadam, S.; Yamanaka, S.; Selaru, F. M.; Shin, E. J.; Kalloo, A. N.; Gracias, D. H. Biopsy with Thermally-Responsive Untethered Microtools. *Adv. Mater.* **2013**, *25* (4), 514−519.
(15) Smith, E. J.; Schulze, S.; Kiravittaya, S.; Mei, Y.; Sanchez, S.; Schmidt, O. G. Lab-in-a-Tube: Detection of Individual Mouse Cells for Analysis in Flexible Split-Wall Microtube Resonator Sensors. *Nano Lett.* **2011**, *11* (10), 4037−4042.
(16) Zakharchenko, S.; Puretskiy, N.; Stoychev, G.; Waurisch, C.; Hickey, S. G.; Eychmüller, A.; Sommer, J.-U.; Ionov, L. Stimuli-Responsive Hierarchically Self-Assembled 3D Porous Polymer-Based Structures with Aligned Pores. *J. Mater. Chem. B* **2013**, *1* (13), 1786−1793.
(17) Mei, Y.; Thurmer, D. J.; Deneke, C.; Kiravittaya, S.; Chen, Y.-F.; Dadgar, A.; Bertram, F.; Bastek, B.; Krost, A.; Christen, J.; Reindl, T.; Stoffel, M.; Coric, E.; Schmidt, O. G. Fabrication, Self-Assembly, and Properties of Ultrathin AlN/GaN Porous Crystalline Nanomembranes: Tubes, Spirals, and Curved Sheets. *ACS Nano* **2009**, *3* (7), 1663−1668.
(18) Silverberg, J. L.; Evans, A. A.; McLeod, L.; Hayward, R. C.; Hull, T.; Santangelo, C. D.; Cohen, I. Using Origami Design Principles to Fold Reprogrammable Mechanical Metamaterials. *Science* **2014**, *345* (6197), 647−650.
(19) Morales, D.; Palleau, E.; Dickey, M. D.; Velev, O. D. Electro-Actuated Hydrogel Walkers with Dual Responsive Legs. *Soft Matter* **2014**, *10* (9), 1337−1348.
(20) Schwaiger, S.; Bröll, M.; Krohn, A.; Stemmann, A.; Heyn, C.; Stark, Y.; Stickler, D.; Heitmann, D.; Mendach, S. Rolled-Up Three-Dimensional Metamaterials with a Tunable Plasma Frequency in the Visible Regime. *Phys. Rev. Lett.* **2009**, *102* (16), 163903.
(21) Smith, E. J.; Liu, Z.; Mei, Y. F.; Schmidt, O. G. System Investigation of a Rolled-up Metamaterial Optical Hyperlens Structure. *Appl. Phys. Lett.* **2009**, *95* (8), 083104.
(22) Peraza-Hernandez, E. A.; Hartl, D. J.; Malak, R. J., Jr.; Lagoudas, D. C. Origami-Inspired Active Structures: A Synthesis and Review. *Smart Mater. Struct.* **2014**, *23* (9), 094001.
(23) Liu, F.; Urban, M. W. Recent Advances and Challenges in Designing Stimuli-Responsive Polymers. *Prog. Polym. Sci.* **2010**, *35* (1−2), 3−23.
(24) Bassik, N.; Abebe, B. T.; Laflin, K. E.; Gracias, D. H. Photolithographically Patterned Smart Hydrogel Based Bilayer Actuators. *Polymer* **2010**, *51* (26), 6093−6098.
(25) Na, J.-H.; Evans, A. A.; Bae, J.; Chiappelli, M. C.; Santangelo, C. D.; Lang, R. J.; Hull, T. C.; Hayward, R. C. Programming Reversibly Self-Folding Origami with Micropatterned Photo-Crosslinkable Polymer Trilayers. *Adv. Mater.* **2015**, *27* (1), 79−85.
(26) Mu, X.; Sowan, N.; Tumbic, J. A.; Bowman, C. N.; Mather, P. T.; Qi, H. J. Photo-Induced Bending in a Light-Activated Polymer Laminated Composite. *Soft Matter* **2015**, *11* (13), 2673−2682.
(27) Tolley, M. T.; Felton, S. M.; Miyashita, S.; Aukes, D.; Rus, D.; Wood, R. J. Self-Folding Origami: Shape Memory Composites Activated by Uniform Heating. *Smart Mater. Struct.* **2014**, *23* (9), 094006.
(28) Suzuki, K.; Yamada, H.; Miura, H.; Takanobu, H. Self-Assembly of Three Dimensional Micro Mechanisms Using Thermal Shrinkage of Polyimide. *Microsyst. Technol.* **2007**, *13* (8−10), 1047−1053.
(29) Yoon, C.; Xiao, R.; Park, J.; Cha, J.; Nguyen, T. D.; Gracias, D. H. Functional Stimuli Responsive Hydrogel Devices by Self-Folding. *Smart Mater. Struct.* **2014**, *23* (9), 094008.
(30) Jamal, M.; Zarafshar, A. M.; Gracias, D. H. Differentially Photo-Crosslinked Polymers Enable Self-Assembling Microfluidics. *Nat. Commun.* **2011**, *2*, 527.
(31) Zhang, Y.; Ionov, L. Actuating Porous Polyimide Films. *ACS Appl. Mater. Interfaces* **2014**, *6* (13), 10072−10077.
(32) Fuchi, K.; Ware, T. H.; Buskohl, P. R.; Reich, G. W.; Vaia, R. A.; White, T. J.; Joo, J. J. Topology Optimization for the Design of Folding Liquid Crystal Elastomer Actuators. *Soft Matter* **2015**, *11* (37), 7288−7295.
(33) Tabiryan, N.; Serak, S.; Dai, X.-M.; Bunning, T. Polymer Film with Optically Controlled Form and Actuation. *Opt. Express* **2005**, *13* (19), 7442.
(34) Podgórski, M.; Nair, D. P.; Chatani, S.; Berg, G.; Bowman, C. N. Programmable Mechanically Assisted Geometric Deformations of Glassy Two-Stage Reactive Polymeric Materials. *ACS Appl. Mater. Interfaces* **2014**, *6* (9), 6111−6119.
(35) Ryu, J.; D'Amato, M.; Cui, X.; Long, K. N.; Qi, H. J.; Dunn, M. L. Photo-origami—Bending and Folding Polymers with Light. *Appl. Phys. Lett.* **2012**, *100* (16), 161908.
(36) Felton, S.; Tolley, M.; Demaine, E.; Rus, D.; Wood, R. A Method for Building Self-Folding Machines. *Science* **2014**, *345* (6197), 644−646.
(37) Behl, M.; Razzaq, M. Y.; Lendlein, A. Multifunctional Shape-Memory Polymers. *Adv. Mater.* **2010**, *22* (31), 3388−3410.
(38) Cuevas, J. M.; Rubio, R.; Germán, L.; Laza, J. M.; Vilas, J. L.; Rodriguez, M.; León, L. M. Triple-Shape Memory Effect of Covalently Crosslinked Polyalkenamer Based Semicrystalline Polymer Blends. *Soft Matter* **2012**, *8* (18), 4928.
(39) Liu, Y.; Boyles, J. K.; Genzer, J.; Dickey, M. D. Self-Folding of Polymer Sheets Using Local Light Absorption. *Soft Matter* **2012**, *8* (6), 1764−1769.
(40) Turner, N.; Goodwine, B.; Sen, M. A Review of Origami Applications in Mechanical Engineering. *Proc. Inst. Mech. Eng., Part C* **2016**, *230*, 2345−2362.
(41) Nair, D. P.; Cramer, N. B.; McBride, M. K.; Gaipa, J. C.; Shandas, R.; Bowman, C. N. Enhanced Two-Stage Reactive Polymer Network Forming Systems. *Polymer* **2012**, *53* (12), 2429−2434.
(42) Nair, D. P.; Cramer, N. B.; Gaipa, J. C.; McBride, M. K.; Matherly, E. M.; McLeod, R. R.; Shandas, R.; Bowman, C. N. Two-Stage Reactive Polymer Network Forming Systems. *Adv. Funct. Mater.* **2012**, *22* (7), 1502−1510.
(43) Landini, G. *ThreePointCircularROI*.
(44) Hill, L. W. Calculation of Crosslink Density in Short Chain Networks. *Prog. Org. Coat.* **1997**, *31* (3), 235−243.
(45) Ye, S.; Cramer, N. B.; Bowman, C. N. Relationship between Glass Transition Temperature and Polymerization Temperature for Cross-Linked Photopolymers. *Macromolecules* **2011**, *44* (3), 490−494.
(46) Timoshenko, S. P.; Goodier, J. N. *Theory of Elasticity*, 3rd ed.; McGraw−Hill: New York, 1970.
(47) Hanna, B. H.; Lund, J. M.; Lang, R. J.; Magleby, S. P.; Howell, L. L. Waterbomb Base: A Symmetric Single-Vertex Bistable Origami Mechanism. *Smart Mater. Struct.* **2014**, *23* (9), 094009.

DOI: 10.1021/acsami.6b08981
ACS Appl. Mater. Interfaces 2016, 8, 29658−29667